

## Fundamental study on post-buckling behavior of reactor vessels under excessive seismic load

Sho Hasegawa<sup>1</sup>, Naoto Kasahara<sup>2</sup>, Masakazu Ichimiya<sup>2</sup>

<sup>1</sup>The University of Tokyo, Tokyo, Japan (sho9780@gmail.com)

<sup>2</sup>The University of Tokyo, Tokyo, Japan

### ABSTRACT

The purpose of this study is to clarify the buckling occurrence conditions and post-buckling behavior of reactor vessels under excessive seismic load. Vibration tests and FEM analyses were conducted to investigate the behavior before and after buckling by applying vibration loads to two types of specimens: columns as a basic structural member and thin cylindrical shells with a shape similar to the real reactor vessels. The results showed that after buckling, the natural frequency was lower than the input frequency, which caused a phase delay, and the phase was opposite to the input, which prevented energy from being input, and the shape of the specimen was stable without excessive deformation. However, cracks can initiate in thin-walled cylinders. Identifying the likelihood and location of crack initiation is a future issue.

### INTRODUCTION

Buckling is one of the expected failure modes under excessive seismic load for fast reactor vessels which is thin cylindrical shell. Much research has been done on the buckling of cylindrical shells under seismic loading (for example; Akiyama et al. (1993), Sukhvarsh and Mark (2015), Morteza and Mohammad (2018)). However, post-buckling behavior of thin cylindrical shells under dynamic load are not necessarily clear. Under Beyond Design Basis Events(BDBE), even if buckling occurs, the safety function can be maintained as long as the coolant boundary does not fail. This is the ultimate objective of this study. Therefore, not only the buckling strength but also the post-buckling behavior was investigated. In this study, to clarify the buckling occurrence conditions and post-buckling behavior under vibration load, experiments and FEM analyses were conducted to apply vibration loading to two types of specimens: (1) columns as a basic structural member and (2) thin cylindrical shells with a shape similar to the real reactor vessel to investigate the response behavior before and after buckling.

### BUCKLING BEHAVIOR OF COLUMN UNDER AXIAL VIBRATION LOAD

Buckling tests applying axial vibration load to uniaxially stressed column specimens (Figure 1) were conducted. As the material for the test specimens, lead-antimony alloy that simulates the high temperature properties of the actual reactor vessel material was used. The input acceleration (Figure 2) was set at 8 Hz and the maximum acceleration was varied. The columns were given initial imperfection to adjust the natural frequency to that of actual piping system. As shown in the Figure 3, the right end of the specimen was fixed to the shaking table, while the left end was free only in the vibration direction.

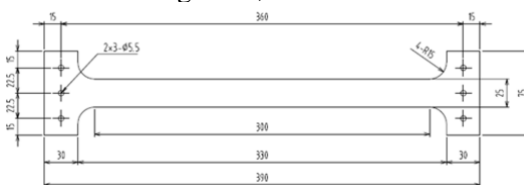


Figure 1. Column dimensions

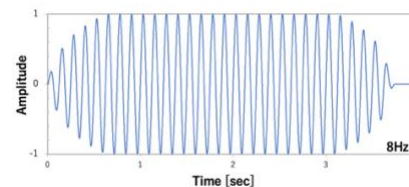


Figure 2. Input acceleration wave

The Figure 4 shows the specimen after the test. As the buckling mode, snap-through buckling occurred. Since Euler buckling occurs under axial compressive static load, the buckling mode is different between dynamic and static load. After buckling, the shape stayed stable without excessive deformation.

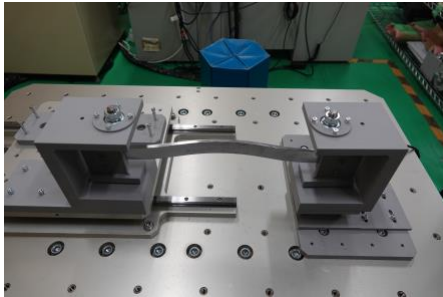


Figure 3. Before buckling

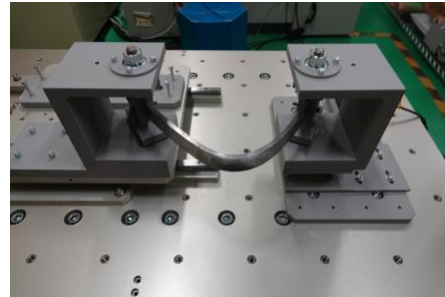


Figure 4. After buckling

The Figure 5 shows the relation between maximum displacement and input acceleration. The acceleration at which buckling occurs is  $25\sim 30\text{ m/s}^2$ . Given that the static buckling load in terms of acceleration is  $6.9\text{ m/s}^2$ , the dynamic buckling load was much higher than the static buckling load. Figure 6 shows the relation between input acceleration and natural frequency, indicating that after buckling, the natural frequency is lower than the input frequency. Figure 7 shows the work rate due to dynamic load. After buckling, the work rate can become negative, indicating that energy is less likely to be input. Such phenomena have already been found in the ratcheting and plastic collapse under vibration load (Lyu et al. (2020), Lyu et al. (2020), Sasaki et al. (2020)).

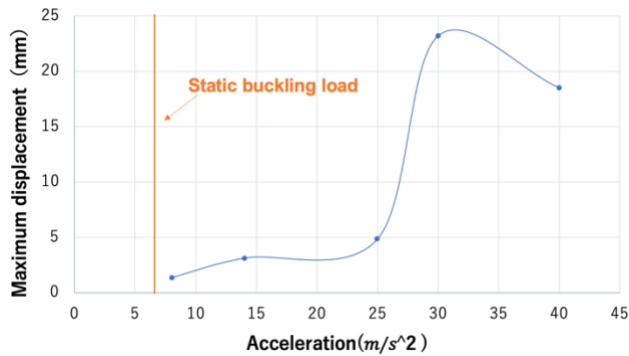


Figure 5. Relation between Acceleration and Maximum displacement

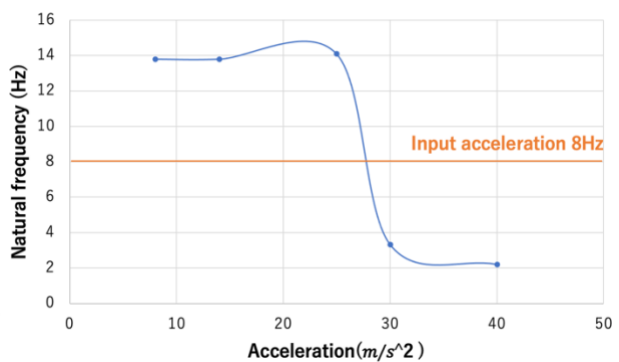


Figure 6. Relation between Acceleration and Natural frequency

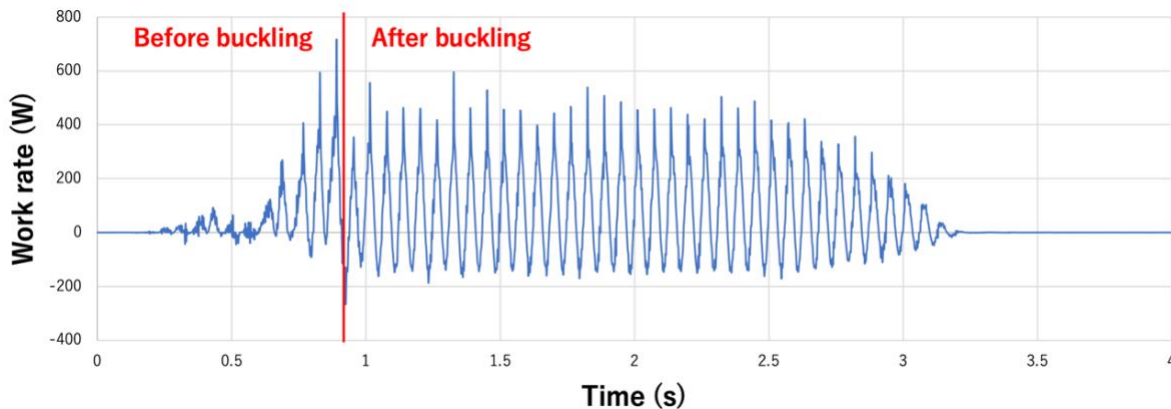


Figure 7. Time-history of the work rate  
**BUCKLING BEHAVIOR OF THIN CYLINDRICAL SHELL UNDER HORIZONTAL VIBRATION LOAD**

*Buckling tests of thin cylindrical shells*

Buckling tests were performed applying horizontal vibration load to carbon steel thin cylindrical shells, simulating the actual reactor vessel. The dimensions are shown in the Table 1. The weight is suspended as shown in the Figure 8. The input acceleration is shown in the Figure 9. The vibration frequency was set at 20 Hz and the maximum acceleration was varied.

Table 1. Specimens' dimensions

Type	Radius (mm)	Length (mm)	Thickness (mm)	Initial natural frequency(Hz) (Number of weights)
L2	26.15	78	0.2	44.69(12)
L3	26.15	78	0.25	39.65(16) 35.06(18)
T2	26.15	52	0.2	54.3(12)
T3	26.15	52	0.25	49.06(16)

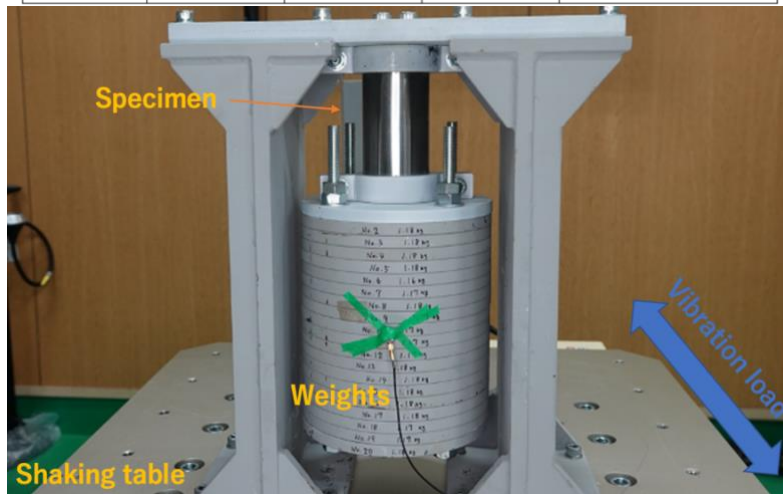


Figure 8. Setup of the vibration test

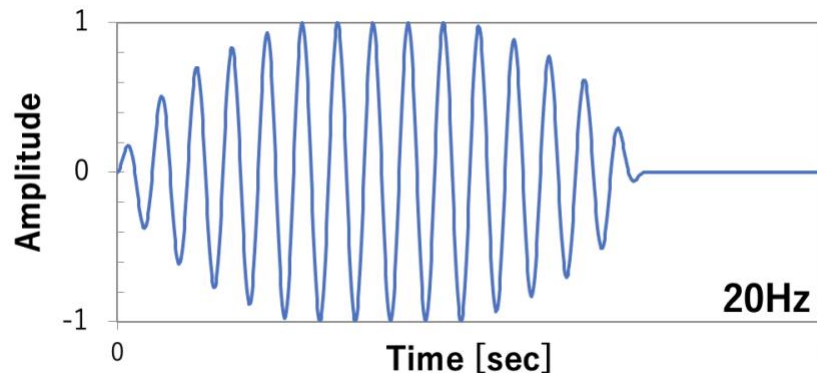


Figure 9. Input acceleration wave

The experimental results are shown in Table 2. The test specimen after the test is shown in Figure 10, 11. In some cases, only deflection occurred as shown in the Figure 10, while in other cases, cracks initiated as shown in the Figure 11. In both cases, the shape stayed stable without excessive deformation in post-buckling. From the observation movies, it was confirmed that the motion of the shaking table and the specimen were in-phase, with both moving in the same direction before buckling, and opposite-phase, with both moving in the opposite direction in post-buckling.

Table 2. Test results

Specimen	Material	Dimensions	Weight	Initial natural frequency	Input acceleration	Buckling acceleration	Post-buckling natural frequency	Post-buckling situation	Date
		mm	number	Hz	Hz	m/s/s	Hz		
L1	Al(A3104)	66Φ100H-0.1t	16	20.21	8(B)	8	-	1α	2021.02.22
L2-1	SPCC	52Φ78H-0.2t	16	34.28	20(A)	20-20-20	20.4->17.8->15.4	2β	2021.10.05
L2-2	SPCC	52Φ78H-0.2t	12	44.69	20(A)	70-70	18.26->11.33	null->3β	2021.12.08
L2-3	SPCC	52Φ78H-0.2t	12	45.16	20(B)	85	6.35	4β	2021.12.14
L2-4	SPCC	52Φ78H-0.2t	12	45.31	20(B)	68	5.96	4β	2021.12.14
L3-1	SPCC	52Φ78H-0.25t	16	39.65	20(A)	75	6.64	1β	2021.11.10
L3-2	SPCC	52Φ78H-0.25t	18	35.06	20(B)	68	2.44	4β	2021.11.17
L3-3	SPCC	52Φ78H-0.25t	18	35.16	12(B)	50	12.5	2α	2021.11.18-1
L3-4	SPCC	52Φ78H-0.25t	18	34.38	20(A)	49	19.34	1α	2021.11.18-2
L3-5	SPCC	52Φ78H-0.25t	16	39.22	20(A)	64	21.97	null	2021.12.09
L4-1	SUS304	52Φ78H-0.3t	18	35.7	20(A)	55	16.99	1α	2022.02.10
L4-2	SUS304	52Φ78H-0.3t	18	35.6	20(A)	50	18.55	1α	2022.03.01
M2	SPCC	52Φ52H-0.2t	12	54.3	20(A)	115	13.6	1α+1β	2021.12.08
M3	SPCC	52Φ52H-0.25t	16	49.06	20(A)	108	11.6	2β	2021.12.09
S4-1	SUS304	52Φ26H-0.3t	18	51.1	20(A)	80	11.71	1α	2022.03.01
S4-2	SUS304	52Φ26H-0.3t	16	56.1	20(A)	100	16.9	1α	2022.03.10

Note)  
 (A); Gradual increase 5 cycles – constant 5 cycles - gradual decrease 5 cycles  
 (B); Gradual increase 5 cycles - constant 15 cycles - gradual decrease 5 cycles  
 null; no visible cracks  
 α; Cracks initiate at the endpoint of the buckling deflection.  
 β; Cracks initiate connected between the endpoints of the buckling deflection.  
 Numbers before α and β are the number of cracks

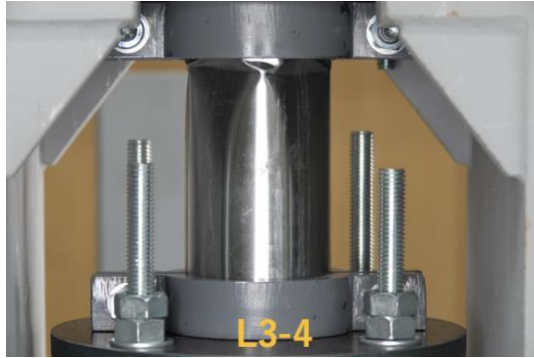


Figure 10. Deformation after buckling without crack initiation

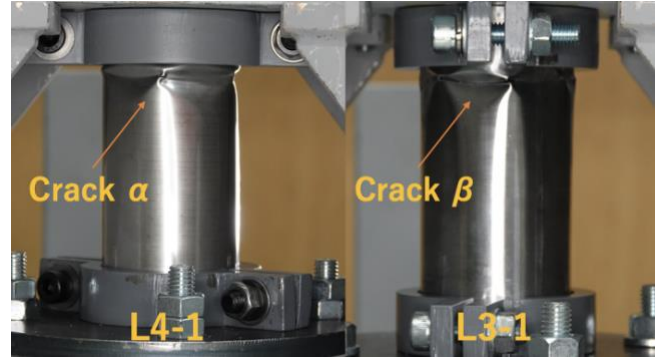


Figure 11. Deformation after buckling with crack initiation

The buckling mode was elephant-foot pattern when the deformation was small and diamond pattern when the deformation was large (Figure 12). Both modes formed at the top of the cylinder. The transition of the buckling mode from elephant-foot to diamond-pattern was also observed in the static compression test (Figure 13).

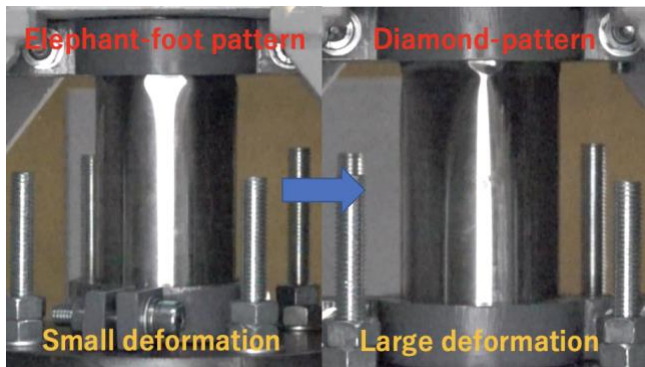


Figure 12. Mode transition during vibration tests

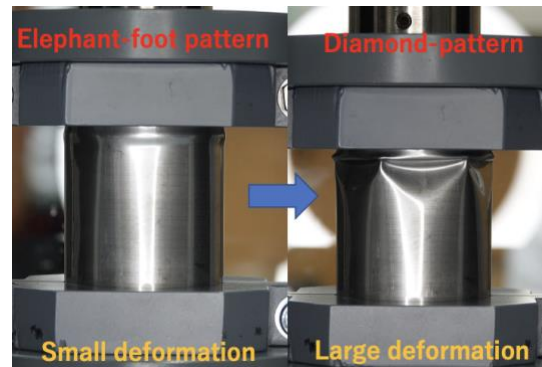


Figure 13. Mode transition during static compression test

Detailed results for L3-4 are presented below as a representative example. The natural frequency of L3-4 was 34.38 Hz before buckling and 19.34 Hz after buckling. Figure 14 shows the response absolute acceleration and Figure 15 shows the relative displacement of L3-4. Figure 16 shows schematically the sequence of the specimen deflection during vibration. Figure 17 shows the restoring force-relative displacement curve. The time-history of response absolute acceleration shows that the response is greatly reduced right after buckling. The time-history of relative displacement are almost equally spaced except between C and E, confirming that a phase delay occurred between C and E. From the observation video, it is only from E that the phase is clearly visible as opposite phase, and at D, there was a little phase delay, but the phase was visible as in-phase from time to time. The large displacement was observed at D despite post-buckling. It is due to the fact that the phase delay is still occurring between C and D and the energy input is large because there are many in-phase period zones. This estimation is supported by the analyses described below.

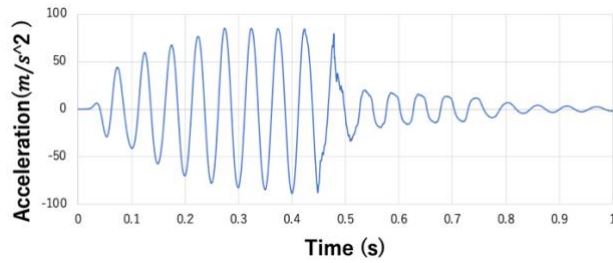


Figure 14. Time-history of response absolute acceleration

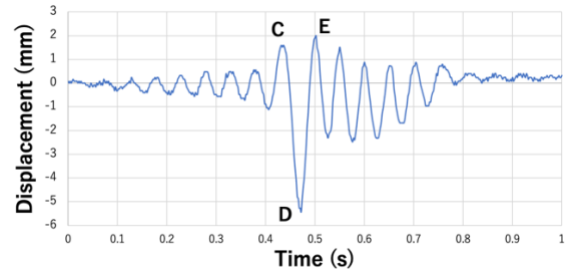


Figure 15. Time-history of relative displacement

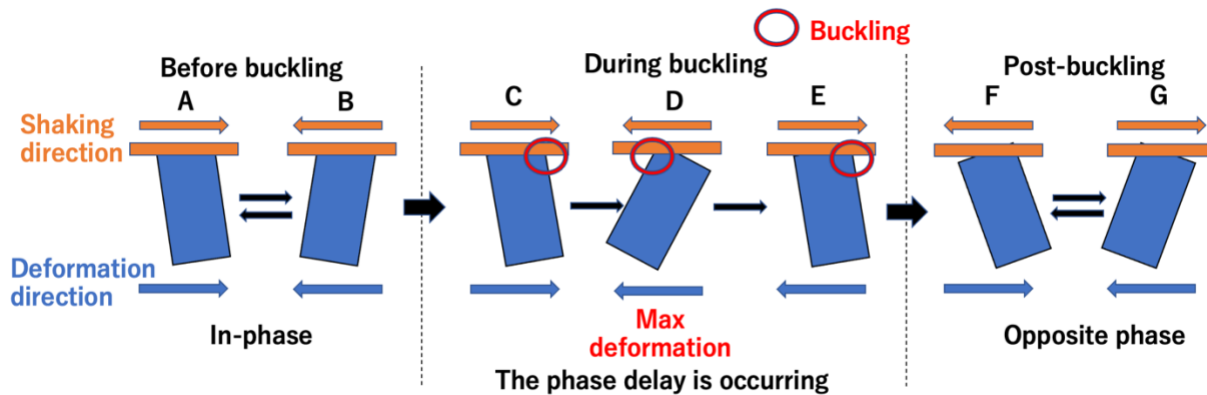


Figure 16. The sequence of the specimen deflection during vibration

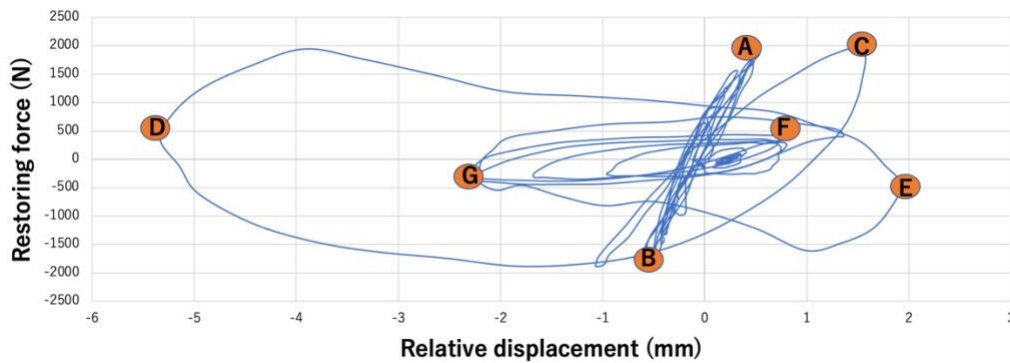


Figure 17 The restoring force-relative displacement curve

Figure 18 shows the natural frequencies before and after buckling and Figure 19 shows the phase delay after buckling. It was also confirmed in other specimens that the natural frequency dropped significantly, and was equal to or lower than the input frequency of 20 Hz, and that a phase delay was observed after buckling. The larger the maximum relative displacement, the greater the decrease in natural frequency and the closer the phase delay to  $\pi$ .

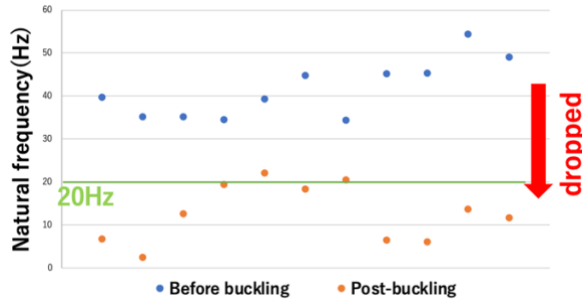


Figure 18. Shift in natural frequencies

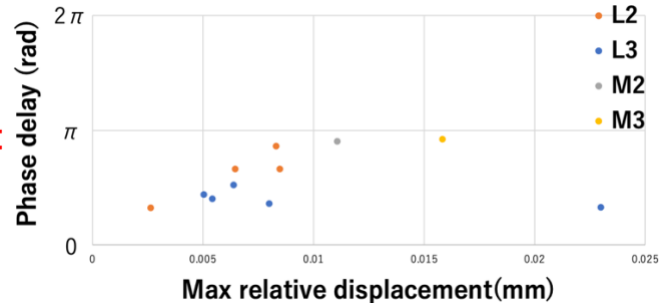


Figure 19. Maximum relative displacement-dependence of Phase delay

The maximum relative displacement and the decrease ratio in response absolute acceleration (the peak value of the response absolute acceleration after buckling,  $A_1$ , divided by the peak value of the response absolute acceleration before buckling,  $A_0$ ) is shown in the Figure 20. The graph shows that when the maximum relative displacement is large, the decrease in absolute acceleration also tends to be large.

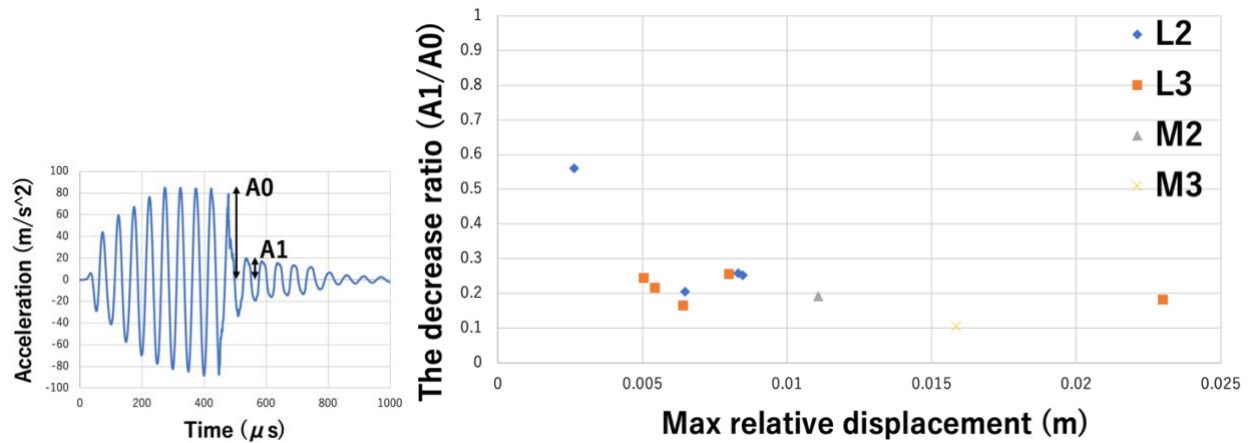


Figure 20. The decrease ratio in response absolute acceleration

From the above, it is concluded that after buckling, the natural frequency decreases and falls below the input frequency, resulting in a phase delay and opposite phase, and energy is less likely to be input from the shaking table. Thus, the shape is stable without excessive deformation. It is also concluded that the greater the maximum relative displacement, in other words, the greater the deformation during buckling, the greater the decrease in natural frequency and phase delay, and the greater the decrease in response absolute acceleration.

### *Analyses of thin cylindrical shells*

FEM analysis was conducted on cylinders with the same geometry and acceleration as in the experiment. The model used is shown in the Figure 21, and the Figure 22 was used as the constitutive equation. The data for each of the models are shown in Table 3.

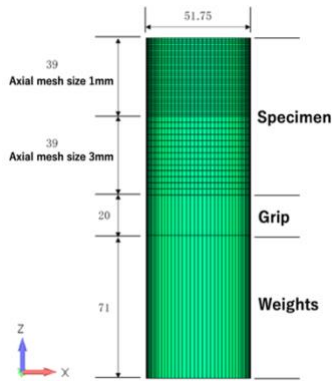


Figure 21. Analyses model

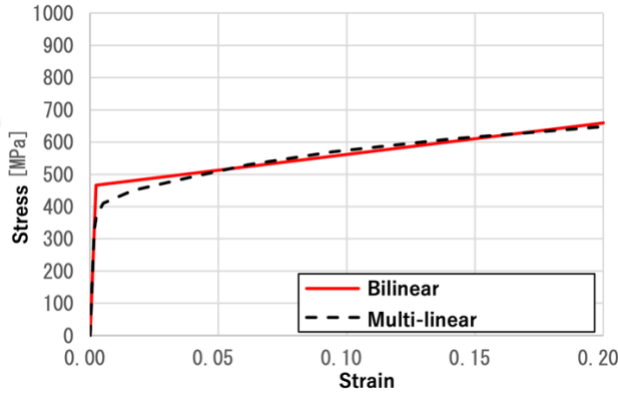


Figure 22. Stress-strain curve

Table 3. Model's data

Young's modulus	133MPa
Poisson's ratio	0.3
Damping ratio	0.1%
Natural frequency	34.38Hz
Weights	22.56kg

The response absolute acceleration, strain concentration contour, restoring force-relative displacement curve and time-history of phase delay obtained by the analyses are shown in Figure 23, 24, 25, 26 respectively. The graphs and diagrams have the same shape as those of the experiments, indicating that the analyses well simulated the experiments.

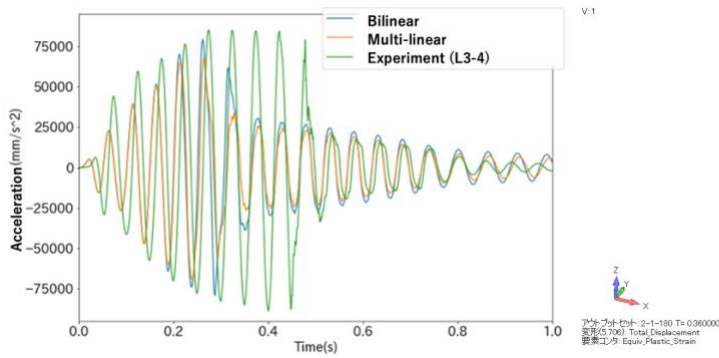


Figure 23. Time-history of response absolute acceleration

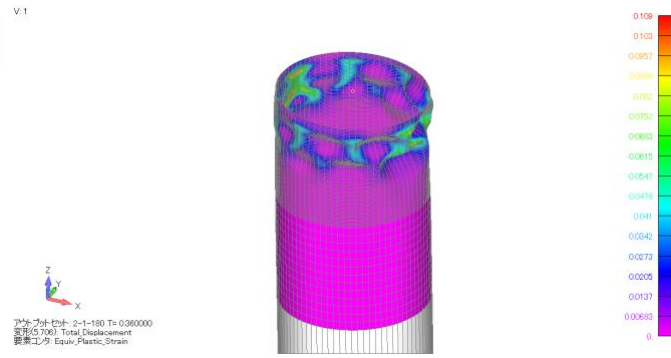


Figure 24. Strain contour

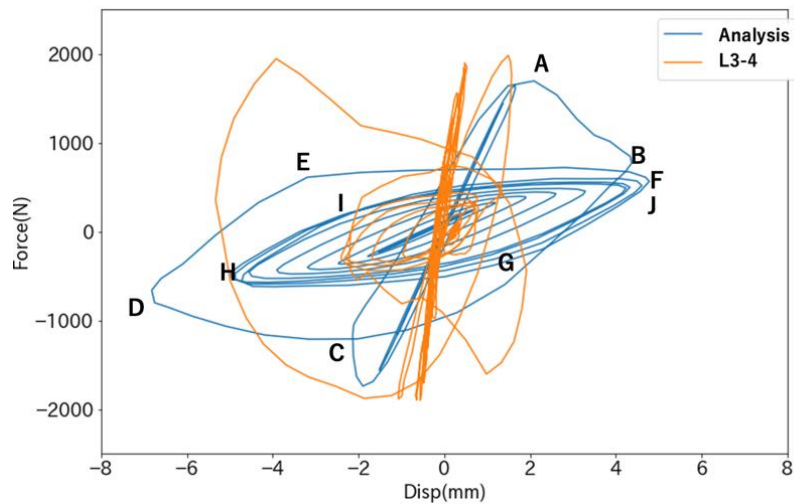


Figure 25. The restoring force-relative displacement curve

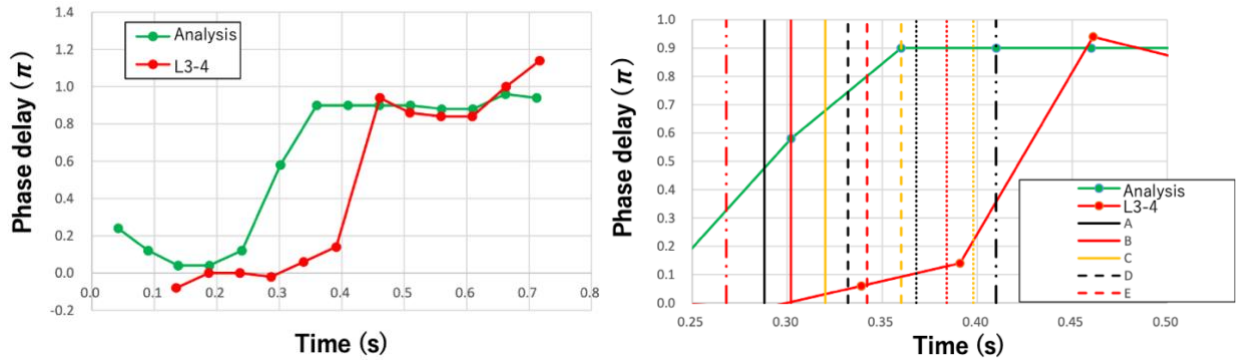


Figure 26. The time-history of Phase delay (left) and its enlarged view (right)

Next, we analysed the energy input to the specimen. When the total weight of the tip load of the specimen is  $m$  and the input acceleration is  $\ddot{x}_e$ , the inertia force (external force) acting on the specimen is  $-\ddot{m}x_e$ . When the response displacement of the gravity center of the weight is  $x$ , the work rate due to the inertia force can be expressed as  $-m\ddot{x}_e\dot{x}$ . Figure 27. shows the work rate. By integrating this over the time of one cycle, the energy input to the specimen in one cycle was calculated. The graph of input energy is shown in Figure 28. The work rate can be negative after buckling, indicating that energy due to dynamic load is less likely to be input.

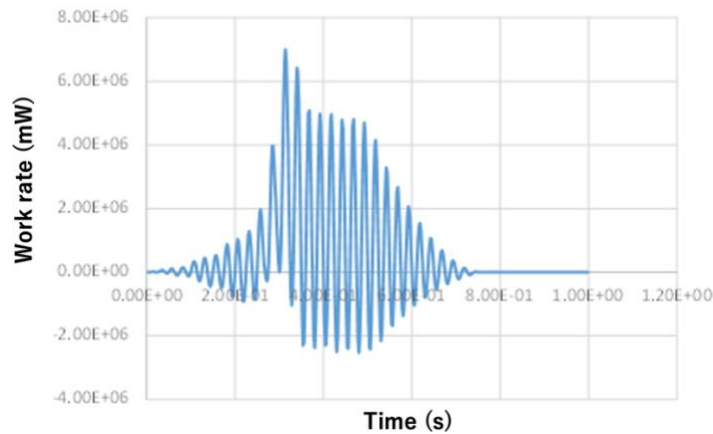


Figure 27. The time-history of the work rate

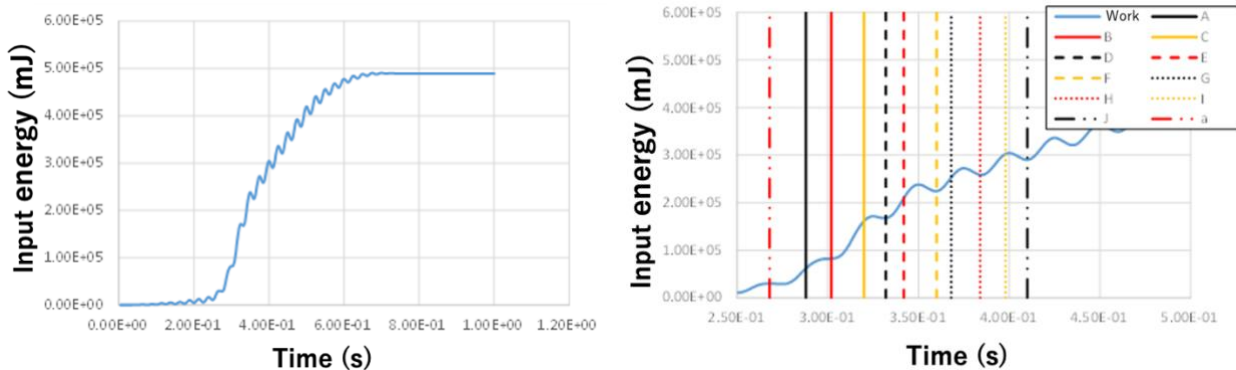


Figure 28. The time-history of Input energy (left) and its enlarged view (right)

## CONCLUSION

The following results were obtained from this study.

- The buckling mode that occurs in the column specimens under dynamic load is snap-through buckling, which is different from the buckling mode under static load. The dynamic buckling load is much higher than the static buckling load, and therefore, buckling due to dynamic load is less likely to occur than buckling due to static load. After buckling, the natural frequency decreases and falls lower than the input frequency, causing the phase shift from in-phase to opposite phase, and energy is less likely to be input.
- The buckling mode of tested cylindrical shells changes from elephant-foot pattern to diamond-pattern depending on the amount of deformation under vibration as well as static loads. In both cases, the shape after buckling is stable.
- In the thin cylindrical shells, the natural frequency dropped lower than the input frequency right after buckling, and phase delay occurred, resulting in opposite phase. Thus, energy was less likely to input, and further deflection was suppressed.
- The vibration analyses of thin cylindrical shells qualitatively simulated the experiment.

## FUTURE WORK

This study shows that cracking is the critical issue for thin cylindrical shells to assure the safety in the post-buckling behavior. Therefore, it is needed to develop a technique to mitigate the propagation of cracks from buckling by clarifying the initiation condition, location, and size of cracks. For this purpose, the followings are needed in the future.

- The test will be conducted using stainless steel specimens, which are the same as the actual materials of reactor vessels.
- FEM analyses will be refined to quantify local strain concentrations. The experimental values of the same area will be investigated using 3D accurate geometry measurement.

## ACKNOWLEDGEMENTS

This work has been sponsored by the Ministry of Education, Culture, Sports, Science and Technology of Japan (MEXT). ITOCHU Techno-Solutions Corporation supports analysis work by FINAS/STAR.

## REFERENCES

- Akiyama H., Ohtsubo H., Nakamura H., Matuura S., Hagiwara Y., Yuhara T., Hirayama H., Kokubo K. and Ooka Y. (1993). "Outline of the seismic buckling design guideline of an FBR - a tentative draft," *Nuclear Engineering and Design* 140, pp319-330.
- Lyu J., Ichimiya M., Sasaki R., Kasahara N. (2020). "Ratcheting occurrence conditions of piping under sinusoidal excitations," *Mechanical Engineering Journal*, Vol. 7(4).
- Lyu J., Ichimiya M., Sasaki R., Kasahara N. (2020). "Study on ratcheting of beams under the combination of gravity and seismic load," *Mechanical Engineering Journal*, Vol. 7(3).
- Morteza M. and Mohammad A. G. (2018). "Seismic damage criteria for a steel liquid storage tank shell and its interaction with demanded construction material," *Bulletin of the New Zealand Society for Earthquake Engineering*, Vol.51, No.2.
- Sasaki R., Ichimiya M., Lyu J., Kasahara N. (2020). "Frequency Dependency of Beam Collapse due to Vibrataion Loads," *Proceedings of ASME PVP 2020*.
- Sukhvarsh J. and Mark L. (2015). "Stability Analysis of Cylindrical Tanks under Static and Earthquake Loading," *Journal of Civil Engineering and Architecture* 9, 2015, pp72-79.